Structure and Electronic Properties of Large Oligomeric Heterometallic 3d/CeIV Polyoxometalates

Olivier Oms, Nishith Maity, Jérôme C. Marrot, Jiahao Yu, Eric Rivière, William E. Shepard, Youven Benseghir, Khadija Talbi, Anne Dolbecq, Minh Huong Ha-Thi, et al.

Structure and Electronic Properties of Large Oligomeric Heterometallic 3d/Ce^{IV} Polyoxometalates

Olivier Oms,[a] Nishith Maity,[b] Jérôme Marrot,[a] Jiahao Yu,[c] Eric Rivière,[d] William Shepard,[e] Youven Benseghir,[a] Khadija Talbi,[a] Anne Dolbecq,[a] Minh-Huong Ha-Thi,[b] Jose-Ramon Galan-Mascaros[c] and Pierre Mialane[a,*]

[a] Institut Lavoisier de Versailles (ILV), UMR 8180, Université Paris-Saclay, Université de Versailles Saint-Quentin en Yvelines, 45 Avenue des Etats-Unis, 78035 Versailles cedex, France.
[b] Université Paris-Saclay, CNRS, Institut des Sciences Moléculaires d'Orsay, 91405, Orsay, France.
[c] Institute of Chemical Research of Catalonia (ICIQ-CERCA), The Barcelona Institute of Science and Technology (BIST), ES-43007 Tarragona, Spain; Departament de Química Física i Inorgànica, Universitat Rovira i Virgili, Marcel. lí Domingo 1, 43007 Tarragona, Spain.
[d] Institut de Chimie Moléculaire et des Matériaux d'Orsay, CNRS, Université Paris-Saclay, Bâtiment Henri Moissan, 19 avenue des Sciences, 91400 Orsay, France.
[e] Synchrotron Soleil, Dept PROXIMA2 A, Saint-Aubin, BP 48, 91192 Gif-sur-Yvette, France.

ABSTRACT: Merging the rich chemistry of Ce(IV) polyoxometalates (POMs) with that of 3d polyanions remains a challenge due to the strong competition between these highly oxophilic lanthanide cations and 3d metallic ions for coordination to lacunary molecular metal oxides. We report herein the characterization of an unprecedented water stable hexameric Ce^{IV}/Co^{II} POM (**$Ce_{12}Co_6$**) made of two $\{(SiW_9)_2Ce_6\}$ units connected to a $\{(SiW_{10})_2Co_6(PO_4)_2\}$ core, which stability in aqueous media has been evidenced. In addition, the pentameric Ce^{IV}/Ni^{II} compound **Ce_6Ni_8** where two $\{PW_9Ni_3W\}$ and a $\{PW_{10}Ni_2\}$ fragments are grafted on a $\{(PW_9)_2Ce_6\}$ moiety has been obtained. Magnetic studies of **Ce_6Ni_8** revealed ferromagnetic interactions between the Ni^{II} centers constituting the $\{Ni_3PW_{10}\}$ fragments, in agreement with the geometry of such trinuclear cluster. Related insoluble barium salts of **$Ce_{12}Co_6$** and **Ce_6Ni_8** were also prepared, allowing their solid-state electrochemical investigations and showing in particular that in **$Ce_{12}Co_6$** both the cobalt, cerium and silicotungstate moieties are electroactive. Finally, photophysical studies demonstrate the formation of long-lived reduced POMs photosensitized by $[Ru(bpy)_3]^{2+}$, suggesting that **$Ce_{12}Co_6$** and **Ce_6Ni_8** could be used as an efficient reservoir of reduction equivalents for photocatalytic reactions.

INTRODUCTION

The chemistry of 3d-4f heterometallic polyoxometalates (POMs) has attracted remarkable interest over the last decade, not only because of the enormous variety of new structures and topologies of these compounds that could result, but also because of their many potential applications, for example in magnetism and catalysis.[1,2] However, very few molecular POMs in which both 3d and 4f metal ions are incorporated *within* the polyoxometalate framework have been reported to date, the number of 1D to 3D species consisting of 3d homometallic entities connected by 4f cations and 4f homometallic molecular oxides connected by 3d metal ions also remaining limited.[1] The difficulty in obtaining a large library of heterometallic molecular POMs can be explained considering that (i) 3d and 4f cations compete for coordination with lacunary POMs, and as a result pure 3d or 4f species can be obtained concomitantly rather than the targeted 3d-4f POMs, and (ii) the combination of rare earth and 3d cations with lacunary POMs often lead to the precipitation of amorphous materials that are not easy to characterize. However, the (photo)[3]-(electro)[4]-catalytic[5] properties of some of the successfully isolated compounds could be investigated, suggesting that the presence of both electron acceptor and donor metallic centers in a single POM framework can confer interesting properties. Nevertheless, most of the obtained species have been synthesized for magnetic purposes, as exemplified by the isolation of the POM-based $\{Dy^{III}Mn^{III}_4\}$[6] and $\{Dy^{III}_{30}Co^{II}_8\}$[7] compounds, both of which were found to be single-molecule magnets. This could explain why very few species incorporating the diamagnetic, electron acceptor Ce^{IV} ion have been characterized, while the chemistry of polyoxometalates incorporating this ion has proved to be very rich as evidenced in particular by the works of Duval and coll.. This group has indeed shown that large oligomeric homometallic POMs based on $\{Ce^{IV}_3\}$,[8] $\{Ce^{IV}_4\}$[9] or $\{Ce^{IV}_6\}$[10,11] building units and with tremendously various topologies can be obtained. Very interestingly, Kortz and coll. also evidenced that large, water stable, cyclic peroxo-Ce^{IV} POM species can be isolated.[12] In contrast, the two 3d-4f heterometallic POMs obtained by Reinoso et al. in presence of this ion only incorporate one Ce^{IV} center. In the $\{Ce^{IV}Cu^{II}_3\}$ molecular compound $[(Ce^{IV}(O_2CCH_3))Cu^{II}_3(H_2O)(B\text{-}\alpha\text{-}GeW_9O_{34})_2]^{11-}$, resulting from the addition of a Ce^{IV} salt to the well-known $[Cu^{II}_4(H_2O)_2(B\text{-}\alpha\text{-}GeW_9O_{34})_2]^{12-}$ Weakley-type POM, a $\{Ce^{IV}Cu^{II}_3\}$ tetranuclear cluster is sandwiched between two $\{GeW_9\}$ units, a Cu^{II} center being substituted by a Ce^{IV} one during the synthetic process.[13] Alternatively, the $\{Ce^{IV}Mn^{IV}_6\}$ $[(\alpha\text{-}P_2W_{16}O_{57}(OH)_2)(Ce^{IV}Mn^{IV}_6O_9(CH_3COO)_8)]^{8-}$ molecular POM, which consists in a divacant Dawson unit capped by a planar Mn_6 hexagon enclosing a cerium cation, was prepared by Fang et al. by reacting the pre-formed $[Ce^{IV}Mn^{IV}_6O_9(O_2CCH_3)_9(NO_3)(H_2O)_2]$ heterometallic precursor with the vacant $[\alpha\text{-}P_2W_{15}O_{56}]^{12-}$ Dawson species.[14] Also, we can note that an additional heterometallic Ce/Mn

compound has been characterized. However, this last compound consists in the co-crystallization of the cerium {(A-β-$SiW_9O_{34})_2Ce^{IV}_4O_2(CH_3COO)_2$} and manganese {(A-β-$SiW_9O_{34})Mn^{III}_3Mn^{IV}O_3(CH_3COO)_3$} tetranuclear POMs,[15] highlighting the great difficulty to gather in a single molecule 3d and cerium(IV) clusters.

Herein we report for the first time on the synthesis and characterization of large Ce^{IV}/3d heterometallic POM systems. The hexameric **$Ce_{12}Co_6$** and pentameric **Ce_6Ni_8** molecular POMs have been obtained from one-pot reactions performed under mild conditions. These two compounds have been fully characterized in the solid state and their behavior in solution investigated. Their magnetic properties have been studied. Electrochemical investigations have also been carried out, while photophysical studies have been performed to investigate potential electron transfer reaction between these heterometallic species and a photosensitizer, namely $[Ru(bpy)_3]^{2+}$.

EXPERIMENTAL SECTION

Synthesis. Na_{10}[A-α-SiW_9O_{34}]·$12H_2O$ and Na_9[A-α-PW_9O_{34}]·$7H_2O$ have been synthesized as previously described.[16] All other chemicals were used as purchased without purification.

$Rb_{24}Na_8$[{(SiW_9O_{34})$Ce_3O_2(OH)_2(H_2O)$}$_2${$SiW_{10}O_{37}Co_2(OH)(PO_4)$}]$_2Co(H_2O)_2Co(H_2O)_4$•$85H_2O$ (**$Ce_{12}Co_6$**). Na_{10}[A-α-SiW_9O_{34}]·$12H_2O$ (500 mg, 0.19 mmol) and $CoCl_2$·$6H_2O$ (38 mg, 0.16 mmol) were dissolved in 10 mL of an aqueous solution of 0.125 M NaOAc (pH 7, acidified with 1 M HCl). Then, $(NH_4)_2Ce(NO_3)_6$ (200 mg, 0.36 mmol) and Na_3PO_4·$12H_2O$ (50 mg, 0.15 mmol) were added as solids, and the pH adjusted to 6.0 with 1 M NaOH. The suspension was heated to 80°C for 20 min, affording a dark orange solution which was cooled to room temperature. After centrifugation, RbCl (150 mg, 1.24 mmol) was added and the mixture stirred at room temperature for 15 min. The obtained solid was filtrated (m = 230 mg), dissolved in 5 mL of 0.125 M NaOAc (pH 7) and let to slowly evaporate. Brown crystals were collected after one night and washed with a 1 M RbCl aqueous solution, ethanol and ether (44 mg, yield 7% vs. W). M.W. = 20 281 g.mol^{-1}. IR: ν (cm^{-1}) = 1050 (w), 1009 (w), 991 (w), 936 (m), 859 (s), 668 (s), 498 (s). EDX: W:Co:Ce:Rb:Na; calculated 56:6:12:24:8; experimental 56:5.4:12.6:22.0:6.8.

Ba_{16}[{(SiW_9O_{34})$Ce_3O_2(OH)_2(H_2O)$}$_2${$SiW_{10}O_{37}Co_2(OH)(PO_4)$}]$_2Co(H_2O)_2Co(H_2O)_4$•$108H_2O$ (**$BaCe_{12}Co_6$**). Crystals of **$Ce_{12}Co_6$** (230 mg, 1.13 10^{-5} mmol) were dissolved in 20 mL of 0.125 M NaOAc (pH 6, acidified with 1M HCl) and added to a 20 mL $BaCl_2$·$2H_2O$ (1 g, 4.09 mmol) pH 6 aqueous solution. The obtained precipitate was filtrated and washed with water, ethanol and ether (180 mg, yield = 76%). M.W. = 20 680 g.mol^{-1}. IR: ν (cm^{-1}) = 1040 (sh), 1008 (w), 993 (w), 936 (m), 864 (s), 662 (s), 495 (s). EDX: W:Co:Ce:Ba; calculated 56:6:12:16; experimental 56:5.1:12.1:18.

$Rb_{20}Na_3$[{$PW_9O_{34}Ni_3(H_2O)_3(OH)_3(WO_3)$}$_2${$(PW_{10}Ni_2(H_2O)_2O_{36}(OH)_2)$($(PW_9O_{34})_2Ce_6(OH)_4O_4$)}]•$60H_2O$ (**Ce_6Ni_8**): Na_9[A-α-PW_9O_{34}]·$7H_2O$ (500 mg, 0.19 mmol) and $NiCl_2$·$6H_2O$ (129 mg, 0.54 mmol) were dissolved in 10 mL of a 1 M NaOAc (pH = 7) solution. $(NH_4)_2Ce(NO_3)_6$ (100 mg, 0.18 mmol) was added as a solid, and the pH adjusted to 7.0 with 1M NaOH. The suspension was heated to 80°C for 30 min, affording a yellow solution which was cooled to room temperature. RbCl (100 mg, 0.83 mmol) was then added and the mixture stirred at room temperature for 1 h. The solution was centrifuged and let to stand at room temperature. The solution was centrifuged again the day after and then let to evaporate slowly. Yellow crystals were collected one day later and washed with a 1 M RbCl aqueous solution, ethanol and ether (86 mg, yield 15% vs. W). M.W. = 16 409 g.mol^{-1}. IR: ν (cm^{-1}) = 1101 (w), 1036 (m), 935 (m), 874 (m), 810 (m), 676 (s), 484 (s). EDX: W:Ni:Ce:Rb:Na; calculated 48:8:6:20:3; experimental 48:9.3:6.6:20.1:2.4.

$Ba_{11.5}$[{$PW_9O_{34}Ni_3(H_2O)_3(OH)_3(WO_3)$}$_2${$(PW_{10}Ni_2(H_2O)_2O_{36}(OH)_2)(PW_9O_{34})_2Ce_6(OH)_4O_4$}]•$80H_2O$ (**$BaCe_6Ni_8$**). **Ce_6Ni_8** (100 mg, 6.09 10^{-3} mmol) was dissolved in 5 mL of water and added to a 5 mL $BaCl_2$·$2H_2O$ (200 mg, 0.82 mmol) pH 6 aqueous solution. The obtained precipitate was filtrated and washed with water, ethanol and ether (80 mg, yield = 79%). M.W. = 16 570 g.mol^{-1}. IR: ν (cm^{-1}) = 1099 (w), 1043 (m), 937 (m), 876 (m), 813 (m), 672 (s), 479 (s). EDX: W:Ni:Ce:Ba; calculated 48:8:6:11.5; experimental 48: 9.9:5.7:12.2.

Physical methods. Infrared (IR) spectra were recorded on a Nicolet 30 ATR 6700 FT spectrometer. Thermogravimetry analyses (TGA) were performed on a Mettler Toledo TGA/DSC 1, STARe System apparatus under air flow (50 mL min^{-1}) at a heating rate of 5°C min^{-1} up to 700°C. UV-vis spectra were recorded on a Perkin Elmer Lambda 750 UV/Vis/NIR spectrometer using a quartz cuvette with a 1 cm long optical pathway. EDX experiments were performed with a Jeol JSM-5800LV Scanning Microscope equipped with an integrated EDX system, which allows, playing on the applied voltage, to analyze samples up to 2 μm from the surface and not only at the surface of the crystals. Magnetic data were collected using a Quantum Design MPMS XL7 SQUID magnetometer. Magnetic susceptibility has been recorded under a magnetic field of 0.1 T.

Nanosecond transient absorption measurements were performed with the setup described previously.[17] Briefly, an OPO pumped by a pulsed nanosecond Nd:YAG laser (EKSPLA) was used to excite the samples. The laser pulse width was ~ 4 ns (energy of about 1-2mJ/pulse) and the pulse frequency was 10Hz. A white light super continuum laser (STM-2-UV LEUKOS) was used as a probe light. The probe laser was operated at a repetition rate of 20 Hz. The probe beam was split by means of a beam splitter that directs one part of beam to the sample cell while the other is directed towards the reference, to monitor spectral energy distribution fluctuations. The transmitted light from the sample enters into the center of the optical fiber (round-to-linear) bundle that goes to a spectrograph (SPEX 270M, Jobin-Yvon) for analysis. The dispersed white light from the spectrograph is detected by an intensified charge coupled device (ICCD) camera PIMAX-4 (Princeton Instrument). Upon varying the delay time between pump and probe, the transient absorption spectra with and without pump can be recorded using Equation: $\Delta A = log_{10}\left(\frac{s^p_{ref}}{s^0_{ref}} \times \frac{s^0_{sample}}{s^p_{sample}}\right)$, where s^p_{ref} and s^0_{ref} are reference spectra with and without pump

respectively while s^{p}_{sample} and s^{0}_{sample} are sample spectra with and without pump respectively. All the measurements were performed under argon saturation using quartz cuvette of dimensions 10 mm x 4 mm.

For the electrochemical characterization in the solid state, the barium salts **$BaCe_{12}Co_6$**/GPO and **$BaCe_6Ni_8$**/GPO (GPO = graphene oxide) were integrated into carbon paste electrodes. These were prepared by ball milling of a mixture of paraffin oil (20 mg), graphite powder (80 mg), and **$BaCe_{12}Co_6$** or **$BaCe_6Ni_8$** (20 mg), respectively. The composites were introduced in a pocket electrode (0.07 cm^2 surface area and 4 mm depth). All electrochemical experiments were performed under ambient conditions with a Bio-Logic VMP3 multichannel potentiostat and implemented with a three-electrode configuration using carbon rod as counter electrode, Ag/AgCl (3 M KCl) as reference electrode, and the pocket working electrode. 1 M H_2SO_4 (pH 0.1) was used as working electrolyte solution. All potentials were measured *vs.* Ag/AgCl and converted to the reversible hydrogen electrode (RHE) reference scale using $E_{RHE} = E_{Ag/AgCl} + 0.21 + 0.059$ pH (V). Cyclic voltammetry (CV) experiments were carried out with 50 mV s^{-1} scan rate.

For **Ce_6Ni_8**, X-ray Diffraction Intensity data collection was carried out with a Bruker D8 VENTURE diffractometer equipped with a PHOTON 100 CMOS bidimensional detector using a high brilliance IμS microfocus X-ray Mo Kα monochromatized radiation (λ = 0.71073 Å). Despite numerous attempts, achieving good resolution factors for the structure of **$Ce_{12}Co_6$** using this diffractometer has proven challenging. In a final effort, crystals of **$Ce_{12}Co_6$** were subjected to synchrotron diffraction single-crystal data collection with a microfocused X-rays on the Proxima 2A beamline (Synchrotron SOLEIL, France, λ = 0.72936 Å),[18] allowing to obtain a good model of the **$Ce_{12}Co_6$** structure. The absorption corrections were based on multiple and symmetry-equivalent reflections in the data sets using the SADABS program[19] based on the method of Blessing.[20] The structures were solved by direct methods and refined by full-matrix least-squares using the SHELX-TL package.[21] The hydrogen atoms were theoretically located on the basis of the conformation of the supporting atoms. The crystallographic data are gathered in Table S1. CCDC –2268425 (**Ce_6Ni_8**) and 2268426 (**$Ce_{12}Co_6$**) contain the supplementary crystallographic data for this paper. These data can be obtained free of charge from The Cambridge Crystallographic Data Centre via www.ccdc.cam.ac.uk/data_request/cif.

RESULTS AND DISCUSSION

Synthesis and Characterizations. **$Ce_{12}Co_6$** has been obtained via a one-pot reaction by mixing at 80°C in a sodium acetate aqueous solution the trivacant POM [A-α-$SiW_9O_{34}]^{10-}$, sodium phosphate and the Co^{II} and Ce^{IV} precursors. The powder obtained after addition of rubidium chloride to the solution cooled to room temperature was recrystallized in sodium acetate (pH 7), affording single crystals. X-ray diffraction studies (see Table S1 for crystallographic data) revealed that **$Ce_{12}Co_6$** is a hexameric compound made of two $\{(SiW_9)_2Ce^{IV}_6\}$ units connected to a $\{(SiW_{10}Co^{II}_2)_2Co^{II}_2(PO_4)_2\}$ fragment (Figure 1). In each $[(SiW_9O_{34})_2Ce_6O_4(OH)_4(H_2O)_2]^{8-}$ unit, six octacoordinated Ce^{IV} centers forming an octahedron are sandwiched between two [A-α-$SiW_9O_{34}]^{10-}$ trivacant POMs, the cerium ions being linked via both oxo and hydroxo ligands ($d_{Ce\text{-}O(H)}$ = 2.10 – 2.51 Å). Besides, the $\{[SiW_{10}O_{37}Co_2(OH)(PO_4)]_2Co(H_2O)_2Co(H_2O)_4\}$ fragment is made of a central Co^{II} ion located on a pseudo inversion center and connected to two [α-$SiW_{10}O_{37}(OH)Co_2]^{7-}$ Keggin polyoxometalates constituted of two $\{W_3O_{13}\}$ and two $\{W_2CoO_{13}\}$ units around an $\{SiO_4\}$ tetrahedron, the cobalt ions being connected via a vertex. In addition, two phosphate groups not only bind these cobalt centers but also cerium cations of the $\{(SiW_9)_2Ce^{IV}_6\}$ fragments. Finally, a sixth cobalt ion is connected both to a $\{SiW_{10}Co_2\}$ unit and a phosphato group, affording the hexameric **$Ce_{12}Co_6$** POM represented at the bottom of Figure 1.

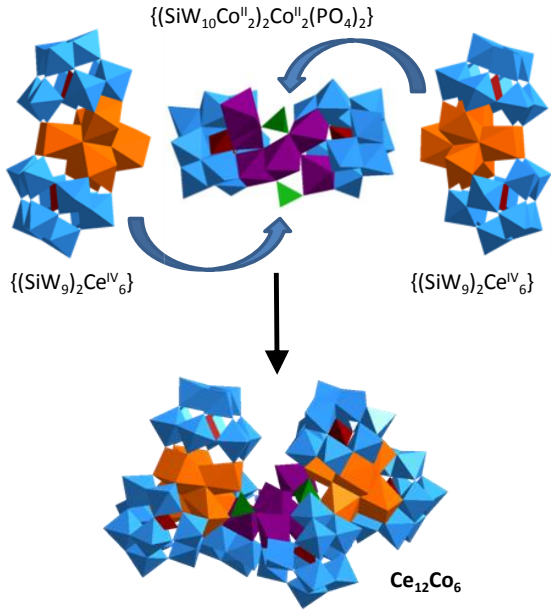

Figure 1. Polyhedral representation of **$Ce_{12}Co_6$** and of its constituting units; blue octahedra, WO_6; orange polyhedra, CeO_8; brown tetrahedra, SiO_4; green tetrahedra, PO_4; purple octahedra, CoO_6.

EDX experiments confirm the metallic composition of the reported heterometallic POM. Its infrared spectrum (Figure 2a) presents the characteristic W=O and W-O_b-W intense bands at wavenumbers below 1000 cm^{-1}, while the bands located at 1050 cm^{-1} and 1009 cm^{-1} can be attributed to P-O vibrations. All these characterizations, combined to TGA experiments (Figure 2b), allow to propose the $Rb_{24}Na_8[\{(SiW_9O_{34})Ce_3O_2(OH)_2(H_2O)\}_2\{SiW_{10}O_{37}Co_2(OH)(PO_4)\}]_2Co(H_2O)_2Co(H_2O)_4 \bullet 85H_2O$ formula for **$Ce_{12}Co_6$**.

$Ce_{12}Co_6$ is poorly soluble in water but can be solubilized in a pH 7 0.125M sodium acetate aqueous solution. Infrared spectrum of the compound dissolved in this medium and re-precipitated with cesium chloride after 30 min at room temperature is analogous to that of pristine **$Ce_{12}Co_6$** crystals (Figure 2a), suggesting that this heterometallic POM is stable in aqueous solution.

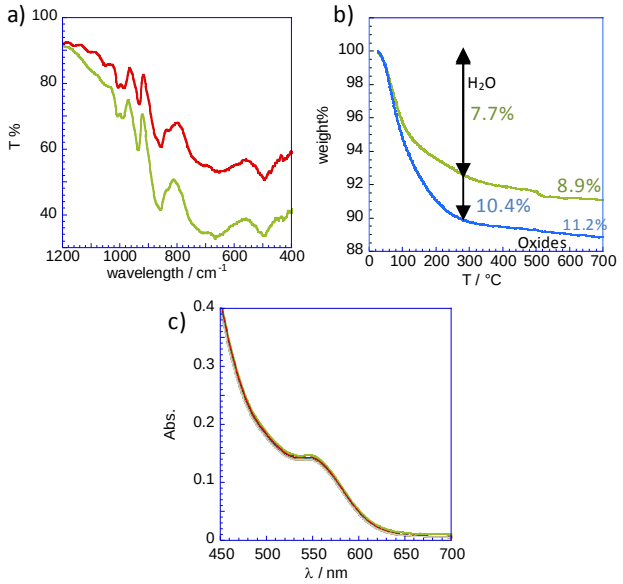

Figure 2. a) IR spectra of pristine **Ce$_{12}$Co$_6$** crystals (green line) and **Ce$_{12}$Co$_6$** dissolved in 0.125 M NaOAc pH 7 and re-precipitated with CsCl (red line); b) TGA measurements of **Ce$_{12}$Co$_6$** (green line) and **BaCe$_{12}$Co$_6$** (blue line); c) UV-Vis spectra of **Ce$_{12}$Co$_6$** (0.125 M NaOAc pH 7, C = 4.2 10^{-4} mol.L^{-1}) recorded every hour in the 0-14 h range.

This is supported by electronic absorption spectroscopy experiments, the visible spectrum of **Ce$_{12}$Co$_6$** dissolved in 0.125 M sodium acetate (pH 7) showing no evolution after 14 hours at room temperature (Figure 2c). Solid-state electronic absorption spectrum of **Ce$_{12}$Co$_6$** (Figure S1) is reminiscent to that obtained in aqueous solution, this last exhibiting d-d transitions at λ = 554 nm and 541 nm, respectively, supporting again the stability of this complex in aqueous solution. Preliminary magnetic studies have been performed on a powdered sample of **Ce$_{12}$Co$_6$**. Related DC susceptibility curves recorded at H = 1000 and 10 000 Oe are represented in Figure S2. When the sample is cooled, the $\chi_M T$ value diminishes from $\chi_M T$ = 21.4 cm^3 mol^{-1} K at 295 K to $\chi_M T$ = 2.85 cm^3 mol^{-1} K at 2 K. The 300-30 K $\chi_M T$ behavior is characteristic of Co^{II} spin-orbit coupling phenomena, the paramagnetic ions in **Ce$_{12}$Co$_6$** possessing a high-spin ground state $^4T_1$ splitted into six anisotropic Kramers doublets. However, at low temperature, the observed decrease can also be due to magnetic anisotropy and exchange interactions between the lowest Kramers doublets of the Co^{II} centers characterized by effective spins S'=1/2, these doublets being the only ones significantly populated at low temperature (typically T < 30K). Concerning the exchange interactions, they could in fact be both of ferromagnetic and antiferromagnetic natures considering that Co-O-Co angles in the 91.5-98.8 and 116.9-126.5° ranges are found in the hexanuclear cobalt cluster constituting **Ce$_{12}$Co$_6$**. Nevertheless, a complete treatment considering the Hamiltonian adapted to the problem would be necessary to confirm this assumption. Besides, it could be noticed that the $\chi_M T$ value determined at room temperature for **Ce$_{12}$Co$_6$** is in good agreement with those previously reported for Co(II) POMs. For example, a $\chi_M T$ value of 37.5 cm^3 mol^{-1} K was found at 300K for the decanuclear Co(II) compound $[Co^{II}_{10}Co^{III}(OH)_5(H_2O)_5(W_6O_{24})(PW_9O_{34})_3]^{22-}$ reported by Duan et al.,[22] leading to $\chi_M T$ = 3.7 cm^3 mol^{-1} K per cobalt ion vs. 3.6 cm^3 mol^{-1} K at 295 K for **Ce$_{12}$Co$_6$**.

The cesium salt of **Ce$_{12}$Co$_6$** obtained above is slightly soluble in water. However, it is known that POM barium salts are fully insoluble in aqueous media.[23] In view to investigate the solid-state electrochemical properties of **Ce$_{12}$Co$_6$** (see below), its alkaline counter-cations have been replaced by Ba^{2+} ions by simply adding $BaCl_2$ to a sodium acetate solution of the title compound, affording **BaCe$_{12}$Co$_6$** as a fully water-insoluble powder. Infrared spectra of **Ce$_{12}$Co$_6$** and **BaCe$_{12}$Co$_6$** are identical (Figure S3). EDX experiments indicate that all the rubidium and sodium cations have been replaced by Ba^{2+}. TGA measurement of **BaCe$_{12}$Co$_6$** (Figure 2b) indicates a weight loss of 11.2% at 700°C - a temperature at which the compound is fully decomposed into oxides -, allowing to determine its molecular weight, which is in agreement with the water content of 10.4% measured at 280°C and allowing to propose $Ba_{16}[\{(SiW_9O_{34})Ce_3O_2(OH)_2(H_2O)\}_2\{SiW_{10}O_{37}Co_2(OH)(PO_4)\}]_2Co(H_2O)_2Co(H_2O)_4 \bullet 108H_2O$ as formula.

Ce$_6$Ni$_8$ has been obtained by heating in water at pH 7 for 30 min the Ni^{II}, Ce^{IV} and $[PW_9O_{34}]^{9-}$ precursors. After cooling down to room temperature, rubidium chloride was added to the yellow solution and single crystals were isolated from the slowly evaporated mother solution. X-Ray diffraction studies (Table S1) revealed that **Ce$_6$Ni$_8$** is a pentameric compound (Figure 3).

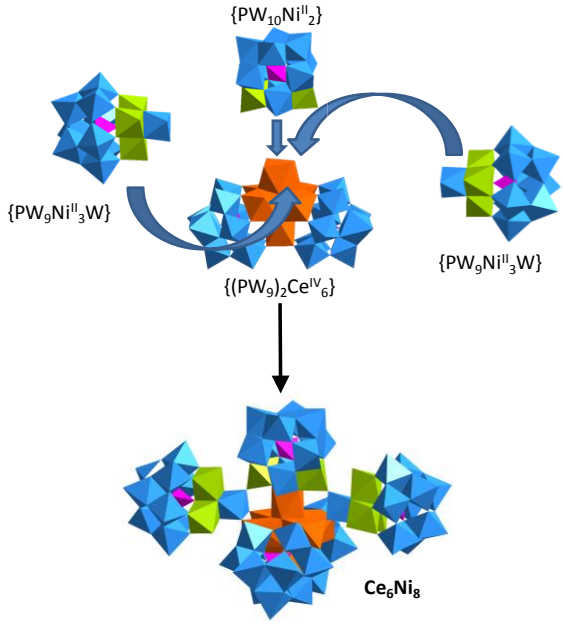

Figure 3. Polyhedral representation of **Ce$_6$Ni$_8$** and of its constituting units; blue octahedra, WO_6; orange polyhedra, CeO_8; purple tetrahedra, PO_4; green octahedra, NiO_6.

Six octacoordinated Ce^{IV} centers sandwiched between two [A-α-$PW_9O_{34}]^{9-}$ POMs form an octahedron highly reminiscent of that found in **Ce$_{12}$Co$_6$** (see above), the cerium ions being also connected via oxo and hydroxo ligands ($d_{Ce\text{-}O(H)}$ = 2.19 – 2.58 Å). One of the cerium ions of the $\{(PW_9O_{34})_2Ce_6(OH)_4O_4\}$ unit ensures a connection to an {α-$PW_{10}Ni_2$} entity in which the nickel centers belong to two adjacent {NiW_2O_{13}} trimetallic triads, the 3d ions being bridged via two {Ni-(O-W-O)$_2$-Ni} and a {Ni-(O-P-O)$_2$-Ni} fragments ($d_{Ni\cdots Ni}$ = 4.76 Å). The resulting trimeric unit

forms an isosceles triangle ($d_{P\cdots P}$ = 8.82 and 10.49 Å) which is sandwiched by two {B–α-PW_9Ni_3W} units, the tungsten atom capping each {PW_9Ni_3} group ensuring connections via two W-O-Ce ($d_{W\cdots Ce}$ = 3.90 and 3.91 Å) and one W-O-Ni ($d_{W\text{-}O\cdots Ni}$ = 3.70 Å) bonds. Such {PW_9Ni_3W} fragment is analogous to that found in the $[Ni_3(H_2O)_3PW_{10}O_{39}H_2O]^{7-}$ compound previously characterized.[24] Overall, it follows that the **Ce_6Ni_8** molecular pentameric compound adopts a pseudo trigonal bipyramidal arrangement. To the best of our knowledge, despite the tremendously huge number of POMs structurally characterized to date, such arrangement is unprecedented in polyoxometalate chemistry.

EDX measurements confirm the W:Ce:Ni metallic ratio in **Ce_6Ni_8**. TGA experiments (Figure S4) indicate a weight loss of 8.1% at 700°C. Considering that the metallic oxides are entirely formed at this temperature, this leads to propose the formula $Rb_{20}Na_3[\{PW_9O_{34}Ni_3(H_2O)_3(OH)_3(WO_3)\}_2\{(PW_{10}Ni_2(H_2O)_2O_{36}(OH)_2)((PW_9O_{34})_2Ce_6(OH)_4O_4)\}]\bullet 60H_2O$ for **Ce_6Ni_8**. The calculated weight loss due to the departure of water molecules (7.5%) is in good agreement with the weight loss observed at 250°C (7.6%). In addition to the W=O (935 cm^{-1}), W-O_b-W (874 cm^{-1}) and W-O_c-W (810 cm^{-1}) bands, the FT-IR spectrum of **Ce_6Ni_8** (Figure S5) exhibits two bands at 1101 and 1036 cm^{-1} which correspond to P-O antisymmetric stretching modes of the phosphotungstate groups.

The magnetic properties of **Ce_6Ni_8** have been investigated and interpreted considering the {$PW_{10}Ni_2$} and the two {PW_9Ni_3W} units as three isolated fragments. Also, the Ni^{II} centers in {$PW_{10}Ni_2$} have been considered as magnetically non-interacting. Figure 4 evidences that the $\chi_M T$ curve exhibits a continuous increase upon cooling from 300 to 10 K, after which $\chi_M T$ rapidly decreases. This is characteristic of a ferromagnetic behavior, in agreement with Ni-O-Ni angles in the 93.5-101.9° range in {PW_9Ni_3W},[25] while the sudden decrease in $\chi_M T$ below 10 K is due to the zero-field splitting (ZFS) effect. The following Hamiltonian has thus been considered:

$$\hat{H} = -2J\,(\hat{S}_1\hat{S}_2 + \hat{S}_2\hat{S}_3 + \hat{S}_3\hat{S}_1 + \hat{S}'_1\hat{S}'_2 + \hat{S}'_2\hat{S}'_3 + \hat{S}'_3\hat{S}'_1) + \sum_{i=1}^{8} \boldsymbol{D}(\hat{S}_z^2 - \hat{S}(\hat{S}+\mathbf{1}))$$

with $S_1 = S_2 = S_3 = S'_1 = S'_2 = S'_3 = 1$ associated to the local spin of the Ni^{II} centers constituting the two {PW_9Ni_3W} units, and the axial ZFS Hamiltonian being relative to the eight Ni^{II} centers present in **Ce_6Ni_8**. The $\chi_M T = f(T)$ and the variation of the magnetization M with the applied magnetic field H in the 0 – 5.5 T range at 2, 3, 4, 6 and 8 K (Figure S6) curves were thus fitted, the best fit parameters obtained being J = +3.8 cm^{-1}, g = 2.27 and D = +6.7 cm^{-1} (Res = 0.019).[26] The determined parameters are in excellent agreement with those extracted from the magnetic data of the related $[Ni_3(H_2O)_3PW_{10}O_{39}H_2O]^{7-}$ POM (J = +3.9 cm^{-1}, g = 2.33 and D = +5.8 cm^{-1}), validating our model.[27]

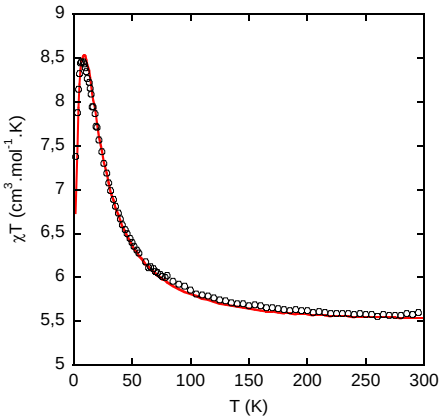

Figure 4. Temperature times magnetic susceptibility per mole of **Ce_6Ni_8** as a function of temperature between 300 and 2 K.

As some small deviations between the fits and the experimental $\chi_M T = f(T)$ and M = f(H) curves are observed at low temperatures (T < 6K), we have attempted to introduce a J' exchange parameter relating the magnetic interaction between the two Ni^{II} centers constituting the {$PW_{10}Ni_2$} unit. The best fit parameters obtained were g = 2.276, D = +6.62 cm^{-1}, J = +3.89 cm^{-1} and J' = -0.349 cm^{-1}. However, only a slight improvement of the low temperature fit was observed (Figure S7). Also, considering the {Ni_3} trinuclear units as isosceles triangles did not significantly improve the fit for T < 6K.

The complex **Ce_6Ni_8** is well soluble in water. Infrared spectrum of the compound dissolved in water and re-precipitated with cesium chloride is analogous to that of pristine **Ce_6Ni_8** crystals (Figure S5). Both the solution (Figure S8) and solid state (Figure S9) electronic spectra evidenced two d-d centered bands in the visible range, with λ = 715 and 749 nm and λ = 721 and 767 nm, respectively. Recording UV-Vis spectra of **Ce_6Ni_8** in solution as a function of time (Figure S8) has highlighted a slight decrease of the absorbance (ca. 6.5% after 1 h) at λ_{max} = 715 nm. Nevertheless, as the observed **Ce_6Ni_8** evolving in solution is slow, a water insoluble salt of **Ce_6Ni_8** has been obtained by readily reprecipitating the alkaline salt of **Ce_6Ni_8** with Ba^{2+}, as performed for **$Ce_{12}Co_6$**. The IR spectrum of the obtained **$BaCe_6Ni_8$** is strictly analogous to that of **Ce_6Ni_8** (Figure S5). Finally, its full formula was determined after TGA (Figure S10) and EDX experiments.

Cyclic voltammetry (CV) experiments in 1 M H_2SO_4 solutions were then conducted to investigate the redox behaviors of **$BaCe_{12}Co_6$** and **$BaCe_6Ni_8$**, respectively (Figure 5).

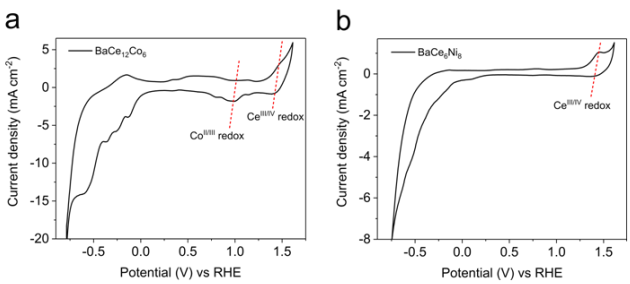

Figure 5. CV curves of (a) **$BaCe_{12}Co_6$**/graphene oxide (GPO) and (b) **$BaCe_6Ni_8$**/GPO in 1 M H_2SO_4.

At negative potentials, both **$BaCe_{12}Co_6$** and **$BaCe_6Ni_8$** functionalized electrodes show multi-electron reduction processes, assigned to multiple electron uptake by $\{XW_9\}$ (X = Si, P) moieties.[28,29,30] The current density reaches maximum values at lowest potential suggesting the concomitant appearance of hydrogen evolution albeit, at very high overpotential. The overall process appears irreversible, since the electron oxidation waves are not observable in the scans towards positive potentials. When positive potentials over 1 V vs RHE are applied, both electrodes show a reversible $Ce^{III/IV}$ wave. This redox wave appears at significantly high oxidation potentials when compared with aqueous $Ce^{III/IV}$, which must be due to electronic withdrawing effects imposed by the POM structure. The major difference between both electrodes resides in the appearance of an additional quasi-reversible Co^{III}/Co^{II} redox peak in **$BaCe_{12}Co_6$**, before and independently of the $Ce^{III/IV}$ event.[31]

To investigate potential electron transfer reaction between these heterometallic species and a photosensitizer (PS), nanosecond transient absorption measurements were performed in samples containing the POM, $[Ru(bpy)_3]^{2+}$ as PS and ascorbate as electron donor by photoexcitation at 460 nm, which correspond to the absorption band of the PS. Transient absorption spectra (TAS) in the presence of **$Ce_{12}Co_6$** together with those of the control experiment in the absence of the POM were recorded at different delay times in pH = 7 acetate solutions (Figure 6). In the absence of POM, photoinduced electron transfer between photoexcited PS and ascorbate produced the reduced PS ($[Ru(bpy)_3]^{+}$) with characteristic transient absorption band at ca. 500 nm rising until 1μs (Figure 6a). At longer delay time, the decay of this transient band reflects the charge recombination between the reduced PS and oxidized ascorbate. The data were fitted globally using a bi-exponential function and the resulted kinetics at selected wavelengths and decays associated difference spectra (DADS) are presented in Figure 6b and Figure S11a, respectively. The first DADS has an associated lifetime of about 170 ns and exhibits a bleaching signal at 460 nm corresponding to the excited state of the PS. The second DADS associated to 38 μs lifetime exhibits absorption maxima at 500 nm and a negative signal at 460 nm, representing the reduced PS.

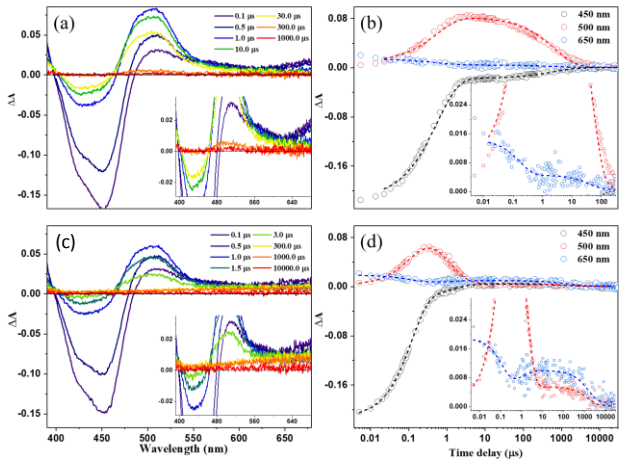

Figure 6. Nanosecond transient absorption spectra and selected kinetic measurements after excitation at 460 nm of $[Ru(bpy)_3]^{2+}$(51 μM) and ascorbate (100 mM) in acetate buffer (pH = 7), (a,b) in the absence and (c, d) in the presence of **$Ce_{12}Co_6$** (100 μM). Inset: corresponding zoomed in Figures.

In the presence of POM, new broad absorption features, tentatively attributed to reduced POM,[32] appeared at longer delay times, from hundreds μs and lives for almost 10 ms (Figure 6c). This is consistent with previous studies which suggested broad and shapeless spectra of reduced POM appearing at particularly longer time delays.[32,33] Kinetics of bleaching signal (450 nm), absorption signals of $[Ru(bpy)_3]^{+}$ (500 nm) and of reduced POM (650 nm) are shown in Figure 6d. Decay of $[Ru(bpy)_3]^{+}$ absorption band at 500 nm is more rapid in the presence of POM, and its disappearance together with the growth of absorption bands at 650 nm of reduced POM (inset of Figure 6d) indicate an electron transfer process from reduced PS to POM. The decays were fitted globally using tri-exponential function yielding DADS shown in Figure S11b. The first and the second time components of 120 ns and 1.4 μs are attributed to decay time of excited and reduced PS, respectively. The longest time component of 1500 μs reflects the lifetime of the reduced POM, corresponding to its recombination with oxidized ascorbate. The mechanism of the formation of reduced POM in $[Ru(bpy)_3]^{2+}$/ascorbate/POM transient absorption experiment is summarized in Figure S12.

In the similar manner, the experiments were also performed under identical conditions using **Ce_6Ni_8**, $[Ru(bpy)_3]^{2+}$ as the photosensitizer and ascorbate as the electron donor in water (Figure S13-S14). The results showed the signature of reduced POM with a lifetime of 732 μs. The detailed discussion of the experiments with **Ce_6Ni_8** can be found in the supplementary information. Overall, these results support the possibility of POM reduction photosensitized by $[Ru(bpy)_3]^{2+}$ for both reported heterometallic POMs.

CONCLUSIONS

We have thus shown here for the first time that it is possible to build oligomeric polyoxometalates associating in a single molecule high-nuclearity cerium(IV) and 3d-substituted POM clusters. Moreover, it has been possible to readily obtain these species under mild conditions via a one-pot synthetic strategy and starting from simple precursors. In the cobalt complex **$Ce_{12}Co_6$**, two $\{(SiW_9)_2Ce_6\}$ units connect a $\{(SiW_{10})_2Co_6(PO_4)_2\}$ core, resulting in a hexameric compound. In contrast, a $\{(PW_9)_2Ce_6\}$ entity constitutes the central unit of the pentameric species **Ce_6Ni_8**, which adopts a unique pseudo trigonal bipyramidal arrangement, the cerium POM cluster being connected to a $\{PW_{10}Ni_2\}$ and two $\{PW_9Ni_3W\}$ fragments. UV-vis and IR studies showed that these high-nuclearity species are stable in aqueous media. Insoluble barium salts of **$Ce_{12}Co_6$** and **Ce_6Ni_8** have also been prepared, and solid-state electrochemical investigations evidenced that in **$Ce_{12}Co_6$** the cobalt, cerium and silicotungstate moieties are electroactive. Moreover, photophysical studies demonstrate the formation of long-lived reduced POM photosensitized by $[Ru(bpy)_3]^{2+}$ for both **$Ce_{12}Co_6$** and **Ce_6Ni_8**, which can thus potentially be used as efficient electron reservoirs. The photocatalytic properties of these new species are currently under study.

ASSOCIATED CONTENT

Supporting Information: Complementary crystallographic, TGA, IR, magnetic, photophysical and electrochemical data (PDF). This material is available free of charge via the Internet at http://pubs.acs.org.

AUTHOR INFORMATION

Corresponding Author

Pierre Mialane - Institut Lavoisier de Versailles (ILV), UMR 8180, Université Paris-Saclay, Université de Versailles Saint-Quentin en Yvelines, 45 Avenue des Etats-Unis, 78035 Versailles cedex, France. E-mail: pierre.mialane@uvsq.fr

Authors

Olivier Oms - Institut Lavoisier de Versailles (ILV), UMR 8180, Université Paris-Saclay, Université de Versailles Saint-Quentin en Yvelines, 45 Avenue des Etats-Unis, 78035 Versailles cedex, France.

Nishith Maity - Université Paris-Saclay, CNRS, Institut des Sciences Moléculaires d'Orsay, 91405, Orsay, France.

Jérôme Marrot - Institut Lavoisier de Versailles (ILV), UMR 8180, Université Paris-Saclay, Université de Versailles Saint-Quentin en Yvelines, 45 Avenue des Etats-Unis, 78035 Versailles cedex, France.

Jiahao Yu - Institute of Chemical Research of Catalonia (ICIQ-CERCA); Departament de Química Física i Inorgànica, Universitat Rovira i Virgili, Marcel. lí Domingo 1, 43007 Tarragona, Spain.

Eric Rivière - Institut de Chimie Moléculaire et des Matériaux d'Orsay, CNRS, Université Paris-Saclay, Bâtiment Henri Moissan, 19 avenue des Sciences, 91400 Orsay, France.

William Shepard – Synchrotron Soleil, Dept PROXIMA2 A, Saint-Aubin, BP 48, 91192 Gif-sur-Yvette, France.

Youven Benseghir - Institut Lavoisier de Versailles (ILV), UMR 8180, Université Paris-Saclay, Université de Versailles Saint-Quentin en Yvelines, 45 Avenue des Etats-Unis, 78035 Versailles cedex, France.

Khadija Talbi - Institut Lavoisier de Versailles (ILV), UMR 8180, Université Paris-Saclay, Université de Versailles Saint-Quentin en Yvelines, 45 Avenue des Etats-Unis, 78035 Versailles cedex, France.

Anne Dolbecq - Institut Lavoisier de Versailles (ILV), UMR 8180, Université Paris-Saclay, Université de Versailles Saint-Quentin en Yvelines, 45 Avenue des Etats-Unis, 78035 Versailles cedex, France.

Minh-Huong Ha-Thi - Université Paris-Saclay, CNRS, Institut des Sciences Moléculaires d'Orsay, 91405, Orsay, France.

Jose-Ramon Galan-Mascaros - Institute of Chemical Research of Catalonia (ICIQ-CERCA; Catalan Institution for Research and Advanced Studies (ICREA), ES-08010 Barcelona, Spain.

Author Contributions

The manuscript was written through contributions of all authors. All authors have given approval to the final version of the manuscript.

Notes

The authors declare no competing financial interest.

ACKNOWLEDGMENTS

This work was supported by the Ministère de l'Enseignement Supérieur et de la Recherche, the Université Paris-Saclay and the Université de Versailles Saint-Quentin and by a grant of the Agence Nationale de la Recherche (ANR-21-CE50-0024). ICIQ-CERCA is supported by the MCIN/AEI/10.13039/501100011033 (CEX2019-000925-S). JRGM thanks the support from the Spanish Ministry of Science and Innovation (PID2021-124796OB-I00), from the Generalitat de Catalunya (2021-SGR-1154), and from the CERCA Programme/Generalitat de Catalunya. J.Y. thanks the China Scholarship Council (CSC) for predoctoral fellowships (File No. 201806270234).

REFERENCES

[1] Das, V.; Kaushik, R.; Hussain, F. Heterometallic 3d-4f polyoxometalates : An emerging field with structural diversity to multiple applications. *Coord. Chem. Rev.* **2020**, *143*, 213271.

[2] Liu, J.; Han, Q.; Chen, L.; Zhao, J. A brief review of the crucial progress on heterometallic polyoxotungstates in the past decade. *CrystEngComm* **2016**, *18*, 842-862.

[3] Chen, Y.; Sun, L.; Chang, S.; Chen, L.; Zhao, J. Synergistic Effect between Different Coordination Geometries of Lanthanides and Various Coordination Modes of 2-Picolinic Acid Ligands Tuning Three Types of Rare 3d−4f Heterometallic Tungstoantimonates. *Inorg. Chem.* **2018**, *57*, 15079−15092.

[4] Li, Y. W.; Li, Y. G.; Wang, Y. H.; Feng, X. J.; Lu, Y.; Wang, E. B. A New Supramolecular Assembly Based on Triple-Dawson-Type Polyoxometalate and 3d−4f Heterometallic Clusters. *Inorg. Chem.* **2009**, *48*, 6452−6458.

[5] Das, V.; Khan, I.; Hussain, F.; Sadakane, M.; Hageo, K.; Ichihashi, K.; Inoue, K.; Nishihara, S. A self-assembled heterometallic {Co7−Ho1} nanocluster: 3d-4f trimeric Keggin-type silicotungstate $[HoCo_7Si_3W_{29}O_{108}(OH)_5(H_2O)_4]^{18-}$ and its catalytic and magnetic applications. *Eur. J. Inorg. Chem.* **2019**, 430−436.

[6] Wu, H.-H.; Yao, S.; Zhang, Z.-M.; Li, Y.-G.; Song, Y.; Liu, Z.-J.; Han, X.-B.; Wang, E.-B. Heterometallic appended $\{MMn^{III}_4\}$ cubanes encapsulated by lacunary polytungstate ligands. *Dalton Trans.* **2013**, *42*, 342−346.

[7] Ibrahim, M.; Mereacre, V.; Leblanc, N.; Wernsdorfer, W.; Anson, C. E.; Powell, A. K. Self-Assembly of a giant tetrahedral 3d-4f Single-Molecule Magnet within a Polyoxometalate system. *Angew. Chem. Int. Ed.* **2015**, *54*, 15574 −15578.

[8] Duval, S.; Trivelli, X.; Roussel, P.; Loiseau, T. Influence of the pH on the Condensation of Tetravalent Cerium Cations in Association with $[\alpha\text{-}SiW_9O_{34}]^{10-}$ Leading to the Formation of a $Ce_6O_4(OH)_4$ Core. *Eur. J. Inorg. Chem.* **2016**, 5373−5379.

[9] Dufaye, M.; Duval, S.; Nursiah, K.; Stoclet, G.; Trivellic, X.; Loiseau, T. Bottom-up synthesis of functionalized $\{Ce_4(SiW_9O_{34})_2(L)_2\}$ polyoxometalates. *CrystEngComm*. **2018**, *20*, 7144-7155.

[10] Dufaye, M.; Duval, S.; Stoclet, G.; Loiseau, T. Influence of pH on Ce^{IV}-$[As^{III}W_9O_{33}]^{9-}$ association for the formation of hexanuclear cerium(IV) oxo-hydroxo-clusters stabilized by trivacant polyanions. *CrystEngComm*, **2020**, *22*, 371-380.

[11] Duval, S.; Roussel, P.; Loiseau, T. Synthesis of a large dodecameric cerium cluster stabilized by the $[SiW_9O_{34}]^{10-}$ polyoxometalate. *Inorg. Chem. Commun.* **2017**, *83*, 52-54.
[12] Qasim, H. M.; Ayass, W. W.; Donfack, P.; Mougharbel, A. S.; Bhattacharya, S.; Nisar, T.; Balster, T.; Solé-Daura, A.; Römer, I.; Goura, J.; Materny, A.; Wagner, V.; Poblet, J. M.; Bassil, B. S.; Kortz, U. Peroxo-Cerium(IV)-Containing Polyoxometalates: $[Ce^{IV}_6(O_2)_9(GeW_{10}O_{37})_3]^{24-}$, a Recyclable Homogeneous Oxidation Catalyst. *Inorg. Chem.* **2019**, *58*, 11300-11307.
[13] Reinoso, S.; Galán-Mascarós, J.R.; Lezama, L. New Type of Heterometallic 3d–4f Rhomblike Core in Weakley-Like Polyoxometalates. *Inorg. Chem.* **2011**, *50*, 9587-9593.
[14] Fang, X.; Kögerler, P. A polyoxometalate-based manganese carboxylate cluster. *Chem. Commun.* **2008**, *29*, 3396–3398.
[15] Fang, X.; McCallum, K.; Pratt III, H.D.; Anderson, T.M.; Dennis, K.; Luban, M. A co-crystal of polyoxometalates exhibiting single-molecule magnet behavior: the structural origin of a large magnetic anisotropy. *Dalton Trans.* **2012**, *41*, 9867–9870.
[16] Ginsberg A. P. Inorganic Syntheses, John Wiley and Sons: New York 1990, *Vol*. 27.
[17] Fatima, A.; Rabah, J.; Allard, E.; Fensterbank, H.; Wright, K.; Burdzinski, G.; Clavier, G.; Sliwa, M.; Pino, T.; Meallet-Renault, R.; Steenkeste, K.; Ha-Thi, M.-H. Selective population of triplet excited states in heavy-atom-free BODIPY-C_{60} based molecular assemblies. *Photochem. Photobiol. Sci.* **2022**, *21*, 1573-1584.
[18] Duran, D.; Couster, S. L.; Desjardins, K.; Delmotte, A.; Fox, G.; Meijers, R.; Moreno, T.; Savko, M.; Shepard, W. PROXIMA 2A – A New Fully Tunable Micro-focus Beamline for Macromolecular Crystallography. *J. Phys.: Conf. Ser.* **2013**, *425*, 012005.
[19] Sheldrick, G. M. SADABS, Program for Scaling and Correction of Area Detector Data, University of Göttingen, Germany, 1997.
[20] Blessing, R. A., Empirical Correction for Absorption Anisotropy. *Acta Crystallogr.* **1995**, *A51*, 33-38.
[21] Sheldrick G. M. SHELX-TL, Software Package for the Crystal Structure Determination, Siemens Analytical X-ray Instrument Division, Madison, WI USA, 1994.
[22] Duan, Y.; Clemente-Juan, J. M.; Giménez-Saiz, C.; Coronado, E. Large Magnetic Polyoxometalates Containing the Cobalt Cubane '$[Co^{III}Co_3{}^{II}(OH)_3(H_2O)_{6-m}(PW_9O_{34})]^{3-}$' (*m* = 3 or 5) as a Subunit. *Front. Chem.* 2018, *6*:231.
[23] See for example Azmani, K.; Besora, M.; Soriano-Lopez, J.; Landolsi, M.; Teillout, A.-L.; de Oliveira, P.; Mbomekallé, I.-M.; Poblet, J. M.; Galán-Mascarós J. R. Understanding polyoxometalates as water oxidation catalysts through iron vs. cobalt reactivity. *Chem. Sci.* **2021**, *12*, 8755-8766.
[24] Gómez-García, C. J.; Coronado, E.; Ouahab, L. A. Novel Polyoxotungstate Containing a triangulo Ni^{II}_3 Cluster with Ferromagnetic Exchange Interactions and an S = 3 Ground State. *Angew. Chem. Int. Ed.* **1992**, *31*, 649-651.
[25] Bertrand, J. A.; Ginsberg, A. P.; Kaplan, R. I.; Kirkwood, C. E.; Martin, R. L.; Sherwood, R. C. Magnetic exchange in transition metal complexes. V. Ferromagnetic spin coupling in a tetranuclear nickel(II) cluster. *Inorg. Chem.***1971**, *10*, 240.
[26] $Res = \left[\sum_{i=1}^{n}(M_{exp} - M_{calc})^2\right]\left[\sum_{i=1}^{n}(\chi_{exp} - \chi_{calc})^2\right]$. Chilton, N. F.; Anderson, R. P.; Turner, L. D.; Soncini A.; Murray K. S. PHI: A powerful new program for the analysis of anisotropic monomeric and exchange-coupled polynuclear *d*- and *f*-block complexes. *J. Comput. Chem.* **2013**, *34*, 1164-1175.
[27] Clemente-Juan, J. M.; Coronado, E.; Galán-Mascarós J. R.; Gómez-García, C. J. Increasing the Nuclearity of Magnetic Polyoxometalates. Syntheses, Structures, and Magnetic Properties of Salts of the Heteropoly Complexes $[Ni_3(H_2O)_3(PW_{10}O_{39})H_2O]^{7-}$,$[Ni_4(H_2O)_2(PW_9O_{34})_2]^{10-}$, and $[Ni_9(OH)_3(H_2O)_6(HPO_4)_2(PW_9O_{34})_3]^{16-}$. *Inorg. Chem.* **1999,** *38,* 55-63.
[28] Arenas, L.F.; Ponce de León, C.; Walsh, F.C. Electrochemical redox processes involving soluble cerium species. *Electrochimica Acta* **2016**, *205*, 226-247.
[29] Swenson, L., Khan, M.I. Electrochemical properties of polyoxometalate composite materials containing multiple redox centers. *Chem. Pap.* **2019**, *73*, 2611-2617.
[30] Boussema, F.; Grossa, A. J.; Hmidac, F.; Ayedc, B.; Majdoubb, H.; Cosniera, S.; Maaref, A.; Holzingera, M. Dawson-type polyoxometalate nanoclusters confined in a carbon nanotube matrix as efficient redox mediators for enzymatic glucose biofuel cell anodes and glucose biosensors. *Biosensors and Bioelectronics* **2018**, *109*, 20-26.
[31] Yu, J., Garcés-Pineda, F.A., González-Cobos, J.; Peña-Díaz, M.; Rogero, C.; Giménez, S.; Chiara Spadaro, M.; Arbiol, J.; Barja, S.; Galán-Mascarós, J.-R. Sustainable oxygen evolution electrocatalysis in aqueous 1 M H_2SO_4 with earth abundant nanostructured Co_3O_4. *Nat Commun.* **2022**, *13*, 4341.
[32] Black, F. A.; Jacquart, A.; Toupalas, G.; Alves, S.; Proust, A.; Clark, I. P.; Gibso, E. A.; Izzet, G. Rapid photoinduced charge injection into covalent polyoxometalate–bodipy conjugates. *Chem. Sci.* **2018**, *9*, 5578-5584
[33] Smortsova, Y.; Falaise, C.; Fatima, A.; Ha-Thi, M.-H.; Méallet-Renault, R.; Steenkeste,K.; Al-Bacha, A.; Chaib, T.; Assaud, L.; Lepeltier, M.; Haouas, M.; Leclerc, N.; Pino, T.; Cadot, E. Time-Resolved Spectroscopy and High-Efficiency Light-Driven Hydrogen Evolution of a $\{Mo_3S_4\}$-Containing Polyoxometalate-Based System. *Chem. Eur. J.*, **2021**, *27*, 17094.

Table of Content Graphic

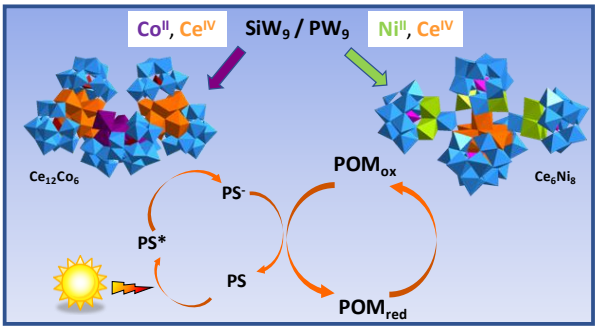

Synopsis

Unprecedented water stable hexameric Ce^{IV}/Co^{II} and pentameric Ce^{IV}/Ni^{II} large polyoxometalates have been synthesized and their magnetic properties investigated. Solid-state electrochemical investigations showed that in the Ce/Co system both the cobalt, cerium and silicotungstate moieties are electroactive, while photophysical studies demonstrate the formation of long-lived reduced POMs photosensitized by $[Ru(bpy)_3]^{2+}$, suggesting that these species could be used as an efficient reservoir of reduction equivalents for photocatalytic reactions.